A&A 423, 849–859 (2004)
DOI: 10.1051/0004-6361:20035804

Astronomy & Astrophysics

Spiral galaxies observed in the near-infrared *K* band⋆,⋆⋆,⋆⋆⋆

I. Data analysis and structural parameters

P. Grosbøl[1], P. A. Patsis[2], and E. Pompei[3]

[1] European Southern Observatory, Karl-Schwarzschild-Str. 2, 85748 Garching, Germany
e-mail: pgrosbol@eso.org
[2] Research Center for Astronomy, Academy of Athens, Anagnostopoulou 14, 10673 Athens, Greece
[3] European Southern Observatory, Alonso de Cordova 3107, Casilla 19001, Santiago 19, Chile

Received 4 December 2003 / Accepted 3 April 2004

Abstract. Deep surface photometry in the *K* band was obtained for 54 normal spiral galaxies, with the aim of quantifying the percentage of faint bars and studying the morphology of spiral arms. The sample was chosen to cover a wider range of morphological types while inclination angles and distances were limited to allow a detailed investigation of the internal structure of their disks and future observations and studies of the disk kinematics. An additional constraint for a well defined subsample was that no bar structure was seen on images in the visual bands. Accurate sky projection parameters were determined from the *K* maps comparing several different methods. The surface brightness distribution was decomposed into axisymmetric components while bars and spiral structures were analyzed using Fourier techniques.
Bulges were best represented by a Sérsic $r^{1/n}$ law with an index in the typical range of 1−2. The central surface brightness of the exponential disk and bulge-to-disk ratio only showed weak correlation with Hubble type. Indications of a central point source were found in many of the galaxies. An additional central, steep, exponential disk improved the fit for more than 80% of the galaxies suggesting that many of the bulges are oblate.
Bars down to the detection level at a relative amplitude of 3% were detected in 26 of 30 galaxies in a subsample classified as ordinary SA spirals. This would correspond to only 5% of all spiral galaxies being non-barred at this level. In several cases, bars are significantly offset compared to the starting points of the main spiral pattern which indicates that bar and spiral have different pattern speeds. A small fraction (∼10%) of the sample has complex central structures consisting of several sets of bars, arcs or spirals.
A majority of the galaxies (∼60%) displays a two-armed, grand-design spiral pattern in their inner parts which often breaks up into multiple arms in their outer regions. Phase shifts between the inner and outer patterns suggest in some cases that they belong to different spiral modes. The pitch angles of the main two-armed symmetric spiral pattern in the galaxies have a typical range of 5−30°. The sample shows a lack of strong, tight spirals which could indicate that such patterns are damped by non-linear, dynamical effects due to their high radial force perturbations.

Key words. galaxies: photometry – galaxies: spiral – galaxies: structure – galaxies: fundamental parameters – infrared: galaxies

1. Introduction

Spiral structure is a prominent feature in most disk galaxies and an important criterion in the Hubble classification of galaxies. It may also be an important factor for the evolution as it can trigger star formation and transfer angular momentum in a galaxy. The appearance of spiral arms in visual bands is dominated by dust and young objects while the old stellar population is emphasized in the near-infrared (Rix & Rieke 1993). Results from optical and NIR observations show significant differences (see e.g. Block & Wainscoat 1991; Block et al. 1994; Grosbøl & Patsis 1998), which indicate that the populations are weakly coupled. The frequency of grand-design, spiral perturbations observed in galactic disks in the *K*-band suggests that a density wave (Lin & Shu 1964, 1966) is the basic, underlying dynamical mechanism for the spiral structure in the majority of disk galaxies.

Although many properties of spiral structure can be observed directly, several questions remain open such as the

⋆ Based on observations collected at the European Southern Observatory, La Silla, Chile; programs: ESO 63.N-0343, 65.N-0287, 66.N-0257.
⋆⋆ Table 2 is only available in electronic form at the CDS via anonymous ftp to cdsarc.u-strasbg.fr (130.79.128.5) or via http://cdsweb.u-strasbg.fr/cgi-bin/qcat?J/A+A/423/849
⋆⋆⋆ Appendix A is only available in electronic form at http://www.edpsciences.org

value of the wave pattern speed (i.e. the location of resonances) and the amplification mechanism. For barred galaxies it has only been possible in a few cases to estimate the pattern speed of bars by direct measurements (see e.g. Merrifield & Kuijken 1995; Laine et al. 1998; Clemens & Alexander 2001) whereas for ordinary spirals it is necessary to rely on indirect means such as associating special morphological features of the pattern to a given resonance (see e.g. Roberts et al. 1975; Contopoulos & Grosbøl 1986; Buta & Purcell 1998).

Another fundamental issue is the importance of bar or oval perturbations in the central regions of galaxies and their relation to spiral structure. Morphological studies in the near-infrared (see e.g. Seigar & James 1998; Eskridge et al. 2000) indicate that the fraction of bars is significantly higher in the infrared than in the visual. The quantitative measure of the distribution of bar strengths in spiral galaxies and its relation to other structural properties is an important issue also for the interaction between bars and spiral arms such as amplification or evolution.

The dispersion relation for density waves in galactic disks (Lin & Shu 1966; Bertin et al. 1989) describes a relationship between the shape of the spiral and global distribution functions of the galaxy such as mass distribution, active mass and velocity dispersion. A detailed comparison between such predictions and the actual shapes of spiral arms would place further constraints on models.

To gain a better understanding of the underlying spiral density wave and its relation to the host galaxy, one needs an accurate description of its morphology together with general properties of the galaxy. Surface photometry in the K'-band enables such accurate mapping of the distribution of the old stellar population in the galaxies without significant attenuation by dust although some population effects are present (Rix & Rieke 1993).

We have selected a sample of nearby spiral galaxies with inclination angles which both allows a full description of the spiral structure and later acquisition of kinematics data for detailed modeling. The sample includes a wide range of morphological types with a subset of ordinary spirals selected to investigate the importance and frequence of weak bars or oval distortions. The current paper describes the data, standard reductions and extraction of structural parameters for the galaxies. This includes the decomposition of the surface brightness into axisymmetric components and characterization of non-axisymmetric perturbations such as bars and spirals. Finally, a brief description of the individual galaxies and a first discussion of the general properties are given. The full discussion of the spiral structure and its relation to the mass distribution of the galaxies will be provided in forthcoming papers.

2. Data and reductions

The total sample consists of 54 non-barred spiral galaxies selected for two separate purposes, namely to study the morphology of spiral structure observed in the K band and to estimate the fraction of bars detectable in the near-infrared for galaxies classified as ordinary in visual bands. All candidates were selected from the Third Reference Catalogue (de Vaucouleurs et al. 1991, hereafter RC3) with inclination angles IA in the range of 25−65° to allow both a good view of the spiral structure and to obtain kinematic information for their disks. Further, a limit on their systemic velocity $V_{\rm GSR} < 5000\ {\rm km\,s^{-1}}$ was imposed to ensure that the linear scale was adequate to study the detailed structure of their spiral pattern. The morphology sample was chosen to cover a wide range of types and absolute magnitudes. It also contains a broad selection of luminosity classes (van den Bergh 1960b,a) and arm classes (Elmegreen & Elmegreen 1987) together with examples of massive and filamentous spirals (Reynolds 1924). The full sample included a subset of 30 ordinary spiral galaxies of which 27 are a part of a complete set of SA galaxies in RC3 with apparent magnitude $m_B < 14.0$, $0.05 < \log(R_{25}) < 0.3$, $1.3 < \log(D_{25}) < 1.9$, $V_{\rm GSR} < 4000\ {\rm km\,s^{-1}}$, $20° < |b_{\rm II}|$, $\delta < 10°$ and within the right ascension interval dictated by the time of observations. All but 6 nearby spirals (IC 5332, NGC 1068, NGC 1566, NGC 2997, NGC 6384 and NGC 7793) had visual diameters $D_{25} < 6'$ so that their disks could be observed with one telescope pointing.

All galaxies were observed in the infrared K' band (Wainscoat & Cowie 1992) with SOFI on the 3.5 m NTT telescope at La Silla, Chile. The galaxies selected for the morphology study were observed mainly in June 1999 and May 2000 while the non-barred sample was observed mostly in November 2000. The data for NGC 2997 and NGC 6118 were acquired during the SOFI commissioning run in 1998 (courtesy of Dr. A. Moorwood). The list of target galaxies is given in Table 1 which also lists morphological type, luminosity class and arm class. A Rockwell Hg:Cd:Te 1024×1024 Hawaii array detector was used with a pixel size of 0.292″ and an exposure time of 60 s per frame subdivided into 6 s integrations. The target exposures were done in a jitter pattern with 5−10″ offsets to ensure that even small groups of bad pixels would not always fall at the same sky position. The exposures on the target were interleaved with different sky fields located typically 10′ from it. The locations of the sky exposures were explicitly selected to avoid bright stars and extended objects. To correct for the rapid variation of the sky conditions in the K band exposures were done in the sequence STTST...TSTTS so that sky frames were taken both before and after each target exposure with a time separation of less than 2 min. The total on-target exposure time varied from 30 min for most of the galaxies in the morphological sample to 10 min for the non-barred sample. The shorter exposure time yielded a sufficiently high signal-to-noise ratio (SNR) in the central parts to detect oval distortions at the level of a few percent while also making it possible to analyze the main part of the spiral structure.

The first step of the reduction was to compare the flat-field exposures made using the dome screen with the median of the sky frames. They were found to be consistent within the errors. Thus, the dome flat field was adopted as it had lower noise. The sky frames were visually compared with each other, and all images with artifacts (e.g. strong sources or uneven backgrounds) were rejected. All point sources were removed by fitting a 2D Gaussian profile to them and subtracting the fitted profiles from the flat field corrected images. The average of the two cleaned sky frames taken just before and after each

target exposure was subtracted from it after which it was divided by the normalized flat field. The corrected frames were then aligned to the nearest full pixel using either the center of the galaxy or nearby stars. This only gave minor alignment errors as the pixel size was significantly smaller than the average seeing. An interpolation of pixel values to a fraction of a pixel was not done as it reduces the ability to remove bad pixels from the image stack. Outliers in the pixel stacks were identified and rejected by testing if the variance of pixels in the stack would be significantly reduced by removing them. This method is more stable than just applying a median filter especially in regions with high gradients such as the center of galaxies. Since each stack contained 10−30 frames, both average and error maps were produced based on the mean and standard deviation computed for the individual pixel stacks. The full-width-at-half-maximum (FWHM) of the seeing derived from 2D Gaussian fits to stars on the final reduced images is given in Table 1.

Standard stars from the list of Persson et al. (1998) were observed frequently during the runs and used to establish the zero point. The weather conditions were unstable during the May 2000 run and the photometric calibration for this run was derived from the aperture photometry of the 2MASS Extended Source Catalog (Jarrett et al. 2000). The error in the *K* band zero point was 0.07 mag for the sample in general. The limiting magnitude for the individual galaxies varied depending on total integration time and observing conditions and was expressed as the surface brightness μ_3 at which $SNR = 3$ per $\square''$ was reached. The quantity μ_3 is given in Table 1 and corresponds roughly to the level where one can detect features with the size of a resolution element. Broader structures like spiral arms can be traced significantly deeper, limited by the stability of the detector and variations of the sky fields e.g. due to faint red background galaxies.

3. Sky projection

Before any analysis was performed, foreground stars were removed by fitting a 2D Gaussian profile with a tilted background to them and then subtracting the profile. This was satisfactory for faint stars while some manual editing was necessary for bright ones. Near to and in the galaxies, only obvious foreground stars were removed and weights in the corresponding areas were appropriately reduced.

The projection parameters of the galaxies on the sky plane (i.e. position angle PA and inclination angle IA) must be determined prior to any analysis of intrinsic properties of the galaxies. Warps and spiral arms in their outer parts make estimates based on simple methods like measurement of axis ratios or ellipticity of outer isophotes less reliable. Three other methods were considered, namely:

– **Constant phase, bisymmetry in disk:** A circular disk will appear elliptical when projected and therefore contain an artificial bisymmetric component with constant phase. By normalizing the disk by its radial mean brightness and performing a 2D Fourier transform in polar coordinates it is possible to determine and minimize the coefficient $A(m = 2, k = 0)$ corresponding to the bisymmetric mode

Table 1. List of target galaxies. Morphological type and luminocity class (L), as given in RC3, are shown together with the arm class (AC), FWHM of seeing on the final image in arcsec, surface brightness μ_3 in mag arcsec^{-2} at which a *SNR* of 3 per $\square''$ was reached, and position angle PA and inclination angle IA both in degrees.

Galaxy	Type	L	AC	seeing	μ_3	PA	IA
IC 438	SAT5	1.6		0.7	20.92	62	44
IC 5020	SAS4	3.3		0.8	20.76	149	37
IC 5041	SXS7	6.7		1.0	21.01	31	62
IC 5332	SAS7	3.9		1.0	20.69	55	25
NGC 157	SXT4	1.8	12	0.7	21.11	37	59
NGC 173	SAT5	2.5	9	0.7	20.76	101	39
NGC 210	SXS3	1.1	6	0.9	20.69	0	59
NGC 470	SAT3	3.6	3	0.8	20.73	176	50
NGC 488	SAR3	1.1	3	0.9	20.77	7	39
NGC 578	SXT5	2.4	9	0.6	20.70	110	56
NGC 685	SXR5	4.0		0.8	20.69	85	18
NGC 787	SAT3	3.1		0.8	20.76	80	35
NGC 895	SAS6	1.9	9	0.6	20.75	111	54
NGC 897	SAT1			0.8	20.79	23	48
NGC 1068	SAT3	2.3	3	0.9	20.74	23	37
NGC 1087	SXT5	5.5	2	0.8	20.68	26	35
NGC 1137	SAT3	4.5		0.7	20.94	29	45
NGC 1255	SXT4	3.3	5	0.8	20.98	117	59
NGC 1309	SAS4	3.4	3	0.8	20.73	11	32
NGC 1357	SAS2		12	0.5	20.74	76	37
NGC 1371	SXT1		4	0.8	21.12	134	42
NGC 1494	SXS7	4.0		0.8	20.79	176	55
NGC 1566	SXS4	1.7	12	0.8	21.02	175	41
NGC 2618	SAT2			0.7	20.72	148	37
NGC 2775	SAR2		3	0.6	20.77	160	35
NGC 2855	SAT0			0.7	20.89	127	37
NGC 2997	SXT5	1.6	9	0.8	20.86	102:	38:
NGC 3054	SXR3	1.5	9	1.0	21.22	117	60
NGC 3173	SAS5	3.7		0.7	20.82	31	30
NGC 3241	SAR2	4.0		0.6	20.78	130	52
NGC 4030	SAS4	1.6	9	0.9	20.73	33	39
NGC 4653	SXT6	3.7	5	1.1	21.21	42	38
NGC 4713	SXT7	4.7	1	1.1	21.22	89	36
NGC 4939	SAS4	1.5	12	1.4	21.17	4	51
NGC 4941	SXR2	3.4	3	1.0	20.79	17	59
NGC 4965	SXS7	4.7	2	0.7	20.57	127	42
NGC 4981	SXR4	3.4	4	0.7	20.30	141	54
NGC 5300	SXR5	3.3	2	0.9	19.60	150	50
NGC 5643	SXT5	4.6		1.5	21.13	80	49
NGC 5688	SXT5	5.6		1.9	20.89	80	61
NGC 5806	SXS3	4.9	5	0.6	20.78	174	65
NGC 6070	SAS6	1.4	9	0.8	20.83	65	63
NGC 6118	SAS6	2.3		1.1	20.86	55	64
NGC 6384	SXR4	1.1	9	0.9	21.02	31	48
NGC 6902	SAR3	3.3		1.1	20.72	148	39
NGC 7070	SAS6	4.8		0.8	20.72	10	44
NGC 7125	SXT5	1.6		1.4	21.23	172	25
NGC 7213	SAS1			0.9	20.31	1	1
NGC 7392	SAS4	2.4	5	0.6	20.77	114	62
NGC 7418	SXT6	3.5		0.8	20.71	122	54
NGC 7637	SAR5	2.2		1.0	20.61	46	23
NGC 7757	SAT5		9	0.9	20.65	130	36
NGC 7793	SAS7	6.9	2	1.0	20.83	106	47
UGC 1167	SAT6			0.9	20.68	113	41

with constant phase and thereby estimate the projection parameters. This method has the advantage of reducing the dependencies on spiral arms and warps since they mostly will contribute to other Fourier components. Further, the radial form of the disk is not assumed. The main source of errors comes from intrinsic bar modes and spherical components like bulges.

– **Fit of 2D exponential disk:** The projection parameters of a spiral galaxy can be estimated by fitting an axisymmetric, exponential disk to the 2 dimensional light distribution of its outer parts which is typically well approximated by this formula. This method may easily be biased by the presence of spiral arms and warps which makes it difficult to apply, especially for open spirals.
– **Phase variation of arms:** The method was described by Danver (1942) and assumes that spiral arms viewed face-on have a smooth phase variation as function of radius. Systematic phase deviations are produced by the projection around major and minor axes and can be used to determine the projection angles. The method works well for tight spirals but may be difficult to apply for open patterns depending on their geometry. For studies of the shape of spirals, like the present, it may introduce an undesirable dependence.
Although this method in principle may yield a good estimate of the projection parameters, it is difficult to apply it in an automatic way as the intersection between the major axis and the spiral arms must be determined.

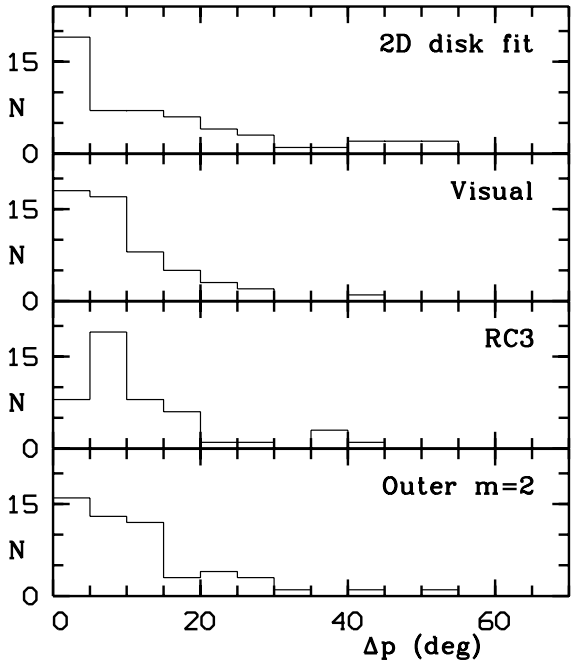

Fig. 1. Histograms of the angular distances between the normals to the plane of the disk estimated by minimizing the bar components in the disk and other determinations (see text) such as **a)** 2D fit of an exponential disk, **b)** visual or interactive estimate, **c)** RC3 projection parameters, and **d)** minimizing the bisymmetric $m = 2$ variation in the outer parts of the disk.

The first two of these methods were applied in the radial region occupied by the main spiral pattern in the galaxies as determined by visual inspection. Since spiral arms typically are located outside the bulge region, this avoids influence from more spherical, central components which otherwise would bias the results. In addition to these methods, the projection parameters were estimated by minimizing the bisymmetric variation in the outer part of the disks as described by Grosbøl (1985) and by visually selecting the "best" parameters viewing a de-projected image for which the projection parameters could be changed interactively. Despite the fact that the latter method is very subjective, it still gives a useful reference as one of the criteria is a smooth radial phase variation of the arms, suggested by Danver (1942).

The first method was preferred as it is based on the middle part of the main disk but is largely independent of the spiral pattern in the galaxies. The distributions of the angular distance Δp between the normal to the galactic disks derived by this method and by the others, including the values given in RC3, are shown in Fig. 1. It is clear that systematic errors due to the morphology of the individual galaxies dominate since typical formal errors are less than a few degrees. If one compares the first two methods (i.e. minimization of bar components and 2D disk fit), a total of 19 galaxies agree to better than 5° while a tail of high residuals may be caused by spiral structure in the disks. The different determinations are consistent within 15° for the majority of the galaxies and suggest that systematic errors are less than 10° in agreement with Barnes & Sellwood (2003) considering additional errors introduced by star forming regions, especially in arm regions, and other non-axisymmetric perturbations.

The projection parameters derived from the first method, minimization of bar modes in the main disk, were adopted for the further analysis and listed in Table 1. For NGC 2997, the parameters obtained from kinematic data (Peterson 1978) were used as a very bright star close to one of its spiral arms made photometric estimates uncertain. Although all references to the galaxies are done as seen face-on, the actual analysis was performed on the original frames. Angles referring to features in the disks were calculated from the northern line of nodes and counted positive eastwards.

4. Axisymmetric properties

The galaxies were decomposed into axisymmetric components for two main reasons: a) to create simple parametric representations of the galaxies which later can be used to generate synthetic rotation curves (Kent 1985), and b) to separate flat and spheroidal components in order to better correct for projection effects caused by different geometries.

The main disks of the galaxies were modeled as single, flat exponential disks without any truncations. The current *K* photometry is not deep enough to justify the use of an outer cut-off of the disk (van der Kruit 1987). Galaxies with strong Type II profiles (Freeman 1970) are less frequently seen in the *K*-band and the excess emission just outside the bulge region for these profiles seems in most cases to originate from sharp features (e.g. young objects) in the arms. Thus, there is no compelling

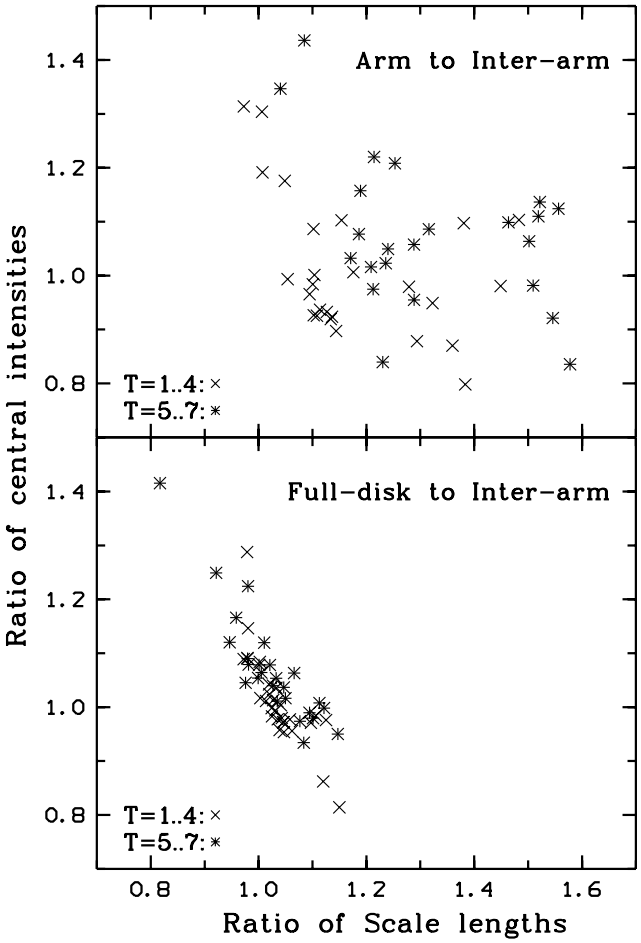

Fig. 2. Ratios of central intensity and scale length obtained by fitting an exponential disk to different parts of the disk. The upper panel show the ratios of fitted values for the arm regions divided by those for the inter-arm regions while the lower diagram displays the values for fits to the full disk over those to the inter-arm regions.

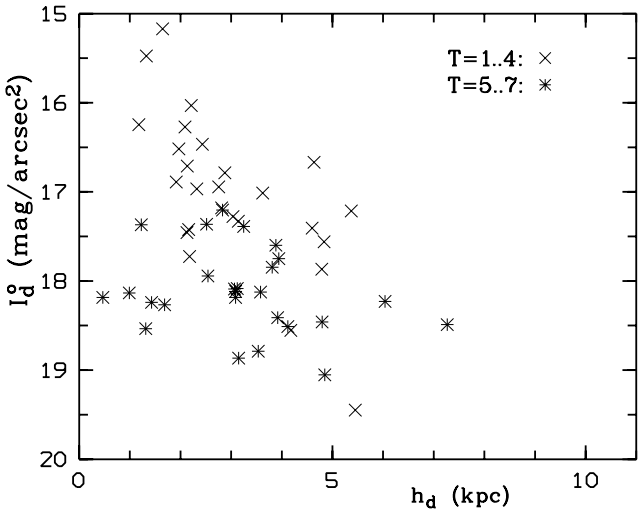

Fig. 3. Distribution of central surface brightness $I_{\rm d}^0$ and linear scale length $h_{\rm d}$ of an exponential disk fitted to the inter-arm regions of the main disk observed in the K' band.

reason for introducing an inner cut-off of the disk which possibly could have improved the formal fit of these galaxies.

The basic decomposition of the surface brightness distribution assumed that each galaxy consisted of three axisymmetric components with a common center, namely: a central point source, a spherical bulge and an exponential disk. Two-dimensional fits were performed in all cases using individual errors from the error maps.

First the main disk was fitted with a single 2D exponential law. The radial range was chosen to coincide with the main spiral pattern in the galaxies as determined above. Although K band maps are less influenced by radiation from young objects than images in bluer colors, extreme population I objects in the spiral arms may still bias the estimate of the disk parameters (Grosbøl & Patsis 1998). To evaluate this effect fits were made to the full disk, and to arm and inter-arm regions, separately. Pixels with an intensity higher than the mean of the minimum and maximum intensities at a given radius were considered as belonging to the arm region. This definition ensures that most pixels associated with bright knots will be grouped in the arm regions. The full disk and arm estimates for central intensity and scale length relative to those obtained for the inter-arm regions are shown in Fig. 2. As the average radius for the estimates is 1−2 scale length, there is a tendency for galaxies with a higher ratio for the scale length to have a lower intensity ratio.

In general, the scale length estimated in the arms is significant longer than that for the inter-arm regions (up to almost 50%) while the mean intensity of the arms is higher, per definition. However because of the longer scale length, the ratio of the central intensities for the disk is in many cases smaller. The distribution displays a large scatter which reflects variations in star formation activity in the arms. On average, late-type spirals have larger scale length ratios than earlier types partly due to more prominent star forming regions at large radii in many late-type systems.

The ratios of full disk to inter-arm estimates show a much tighter relation caused by the relative small influence of the arm regions due to the current definition. Even so, systematic effects of more than 10% are frequent. The inter-arm estimates were adopted to better represent the distribution of the old disk stars as they are less biased by young objects in the arms with significant different mass-to-light ratios. Although the disk scale length derived in this way will give a better estimate, the central intensity will be slightly underestimated.

Distribution of central intensity and scale length for the exponential disks based on the inter-arm regions are listed in Table 2 and shown in Fig. 3. The surface brightness was only corrected for the geometric projection effects since attenuation by dust was assumed to be small. The linear scale for the galaxies was derived from the weighted mean velocity $V_{\rm GSR}$ corrected to the Galactic Standard of Rest as given in RC3 using a Hubble constant of 75 Mpc km s^{-1}. For two galaxies with recession velocities of less than 500 km s^{-1} individual distance moduli were adopted, namely 3.9 Mpc for NGC 7793 (Karachentsev et al. 2003) and 4.2 Mpc for IC 5332 (Bottinelli et al. 1984).

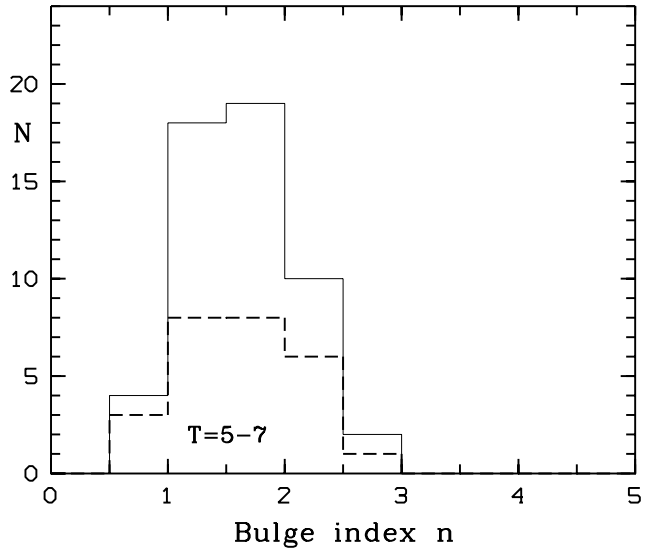

Fig. 4. Histogram of the exponents, $1/n$, in the Sérsic law for bulges where those for galaxies with type $T > 4$ are shown by a dotted line.

The fitted main disk was then subtracted from the K maps before the central components were estimated. The goodness of fit was not good in a strict statistical sense for some 20% of the galaxies. This was largely ascribed to the spiral pattern in the disks which even in the K band is significant. The residuals, after subtracting the disk, were checked visually and confirmed that the fits were acceptable with the spiral pattern being the main deviation.

The region inside the main spiral pattern on the residual maps was first decomposed into two parts, namely a central point source and a spherical bulge. The point source was assumed to be a Gaussian with a width fixed to the value determined for seeing on the same frame. Two mathematical representations for the bulge were tried, namely a modified Hubble law (see Binney & Tremaine 1987), and a Sérsic $r^{1/n}$ power law (Sérsic 1968; Caon et al. 1993) with variable exponent. The fitting procedure convolved the analytical model with the seeing profile before it was compared to the actual map.

The fitting of the central part was acceptable for 27 galaxies while in 9 cases it gave significant residuals. The main reasons were the existence of bar perturbations, hot spots and the detailed shape of the luminosity profile in the very central region. A significant central point source was found in many of the galaxies. A Sérsic law gave the best fit for 36 galaxies while the remaining spirals were better represented by a modified Hubble law. The better fit of the Sérsic law was expected, as it has one more free parameter. The distribution of the power law index n for the bulges is shown in Fig. 4. They lay mostly in the range of 1−2 with no clear trend depending of the morphological type.

It was also tried to add an exponential disk with projection parameters fixed to those of the main galaxy as a third component in the central region. This improved the fits in 46 cases, which could suggests that many of the bulges are oblate. No attempt was made to fit explicit oblate or triaxial models to the bulges since this is ambiguous without additional kinematic data.

The components derived from the best fit were subtracted from the maps to verify the quality visually. In general the residuals were small and mainly showed bar structures or hot spots; however, inside a radius of 2−3″ notable deviations were observed for 8 galaxies. They are likely due to an inadequate representation of the PSF, not being exactly Gaussian, pixel averaging errors in the high gradient regions close to the center and general deviation from the analytic bulge shapes used. Although the general properties of the components will change little due to these residuals, any feature within 2″ of the center cannot be fully trusted.

5. Non-axisymmetric perturbations

The best-fit spherical components, point source and bulge, were subtracted from the K maps before non-axisymmetric variations in the disks were analyzed, to avoid artificial projection effects. The basic analysis of perturbations in the disk was performed using 1D Fourier transforms of the azimuthal variations in 1″ wide annuli. This gave the radial variation of both relative amplitude and phase of each Fourier component upto the 16th harmonic. In some cases, higher harmonics may be important to define the exact shape of sharp features such as strong bars or Population I features (Buta et al. 2003). Weak bars and the main spiral pattern are generally well described by the first 8 harmonics which, on average, contained 85% of the total power assuming a white noise spectrum. Although a 2D Fourier analysis in principle provides more information (e.g. both leading and trailing components), it is sensitive to the radial region within which it is performed. Further, it is more difficult to interpret if the spiral pattern does not follow a simple analytical form such as a logarithmic spiral. Hence, the 1D Fourier technique was used to estimate the basic properties of the spiral arms such as relative amplitude, radial extent and shape.

Although most of the light from galaxies observed in K originates from an old stellar population, one frequently sees strings of very compact objects along the spiral arms (Patsis et al. 2001). Their sizes and alignment suggest that they are young objects. To reduce the influence of such young stellar populations on the estimates of the perturbations in the old disk stars, a median-type digital filter was applied to remove point-like features with a relative amplitude of more than 50% from the maps before the Fourier analysis was performed.

5.1. Bars

Oval distortions and bars are normally associated with radial regions where the bisymmetric ($m = 2$) harmonic has a constant phase although hot spots and strong dust lanes along bars can affect the mean phase as function of radius. Several bars have a smooth transition into the spiral arms (e.g. s-shaped morphology defined by de Vaucouleurs 1959) which makes it difficult to define the end of the bar. Oval distortions and small bars may be fully inside the bulge region which makes it very important to model and subtract the bulge component correctly.

Failing to do this may introduce artificial bar features aligned either along the major or minor axis. Non-spherical bulges and thick disks can give rise to an artificial bar-type morphology which cannot be distinguished from a normal bar without detailed kinematic data. In the main disk, where the spiral pattern is located, the procedure used to estimate the projection parameters will bias against finding oval distortions of the disk itself. Further, warps in the outer disk and errors in the sky background correction may introduce bisymmetric structures with almost constant phase.

Central bars were, in this context, defined as bisymmetric structures with a pitch angle higher than 60° as most spiral arms have pitch angles below 40° (Kennicutt 1981) with very few in the range up to 60°. It was also required that their extent was more than 3″ to ensure that they at least covered 4 radii in the phase diagram. Due to possible residuals from the bulge subtraction in the very center, only bars which could be identified outside a radius of 2″ were considered. The extent of the bar, r_b, was measured manually based on the radial phase and amplitude variation of the second harmonic. The average amplitude A_b of the $m = 2$ term, omitting radii inside 3″, is given in Table 2 together with r_b in terms of the disk scale length.

One possible way to test if the bulge subtraction introduces a bias is to check the distribution of angle distances between the position angle of the main galaxy and of the bar. It is expected to be uniform but would show peaks around 0° or/and 90° if de-projection errors due to the bulge were significant. Using a χ^2 goodness of fit test, the distribution can only be rejected as being uniform on a 30% level which suggests that the determination of bar parameters is not significantly biased by the subtraction of the bulge component. The general noise was estimated from the high order harmonics and suggested that perturbations below a relative amplitude of 3% would not be identified safely.

5.2. Spiral pattern

In the majority of the galaxies a well defined two-armed spiral pattern starts just outside the bar or bulge region. These main spiral arms occupy a major part of the disk but often split up into multiple arms in the outer parts where the pitch angle frequently changes. The radial region of the main spiral was defined manually by both looking on the direct images and the radial phase variation. The outer limit of the main spiral was identified as the radius where the ratio A_4/A_2 of the relative amplitudes of the 4th and 2nd harmonics shows a significant increase, indicating the transition to a multi-armed structure, or where the main arms changed their smooth radial phase variation such as breaking up or alter pitch angle. The pitch angle for the $m = 2$ spiral arms, assuming a logarithmic shape, was estimated by fitting a straight line to the θ–ln(r) phase diagram omitting the inner part of the spiral which often gets more open as it approaches the bar region. Due to the small radial inter-arm distance, it is very difficult to detect tight spirals with an absolute pitch angle $|i_2| < 5°$.

The mean relative amplitude A_2 of the main spiral was calculated in the same region used to estimate the pitch angle. Mean amplitude A_2 and pitch angle i_2 are listed in Table 2 which also shows the strongest or primary spiral mode m_p as derived from the 2D Fourier transform of the region occupied by the main spiral pattern. These quantities can be used to determine the "dust penetrated" classification (Block & Puerari 1999). For many galaxies, the amplitudes varied significantly as function of radius. This is likely due to stellar population changes along the arms where the fraction of young objects varies. Although the effect was reduced by removing point-like objects in the arms regions, there may still be a diffuse component of young stars left. Thus, the relative amplitudes given will be upper limits while the correction will vary from galaxy to galaxy and along the arms depending on the star formation activity. The correlation between amplitudes and phases of the $m = 2$ and 4 modes in the regions of the main spiral also points to population effects being the main cause for the amplitude modulation along the arms rather than interacting wave packages.

6. Discussion

The current set of galaxies was chosen to cover a wide range of morphological types and is not in any strict sense a statistically, well defined sample with clear volume or magnitude limits. Although one cannot directly estimate the true underlying distributions, it is still of interest to look at the variation of the general properties of the galaxies in the total sample.

The central surface brightness I_d^0 of disks in K' has a wide range with an average value of 17.6 ± 0.9 mag arcses^{-2} as seen in Fig. 3. There is a weak dependency on morphological type T (see Fig. 5) where early-type spirals ($T < 5$) show little correlation while late-type galaxies have fainter central brightnesses. This is in good agreement with de Jong (1996b) and Grosbøl (1985) while Seigar & James (1998) find a slightly smaller range and no dependency on Hubble type. The scale length h_d shows no correlation with type and has a typical range of 2−5 kpc with a mean of 3.1 ± 1.4 kpc (see Fig. 3) which corresponds well with de Jong (1996b) and Seigar & James (1998) after adjusting for the different distance scales. Only one galaxy, NGC 5688, with a faint outer disk had $h_d > 6$ kpc. The disk parameters were derived by fitting the inter-arm regions in the main disk of the galaxies to avoid contributions from young objects along the arms and thereby better represent the underlying disk of old stars. The present values of the disk central surface brightness are therefore ~0.05 mag fainter than expected for the average old disk population assuming a constant amplitude of the spiral of 10%. The scale lengths estimated in this way tend to be slightly smaller than those derived from a fit to the whole disk (Grosbøl & Patsis 1998). Neither the scale length itself nor the difference between the estimates, which mainly depends on the amount of young objects in the spiral arms, show any correlation with Hubble type. The scale length shows a weak anti-correlation with the central surface brightness (see Fig. 3) in the sense that centrally bright disks typically have shorter scale lengths than fainter ones in agreement with de Jong (1996b).

The central region was allowed to consist of a point source and a spheroidal component while a flat exponential disk with

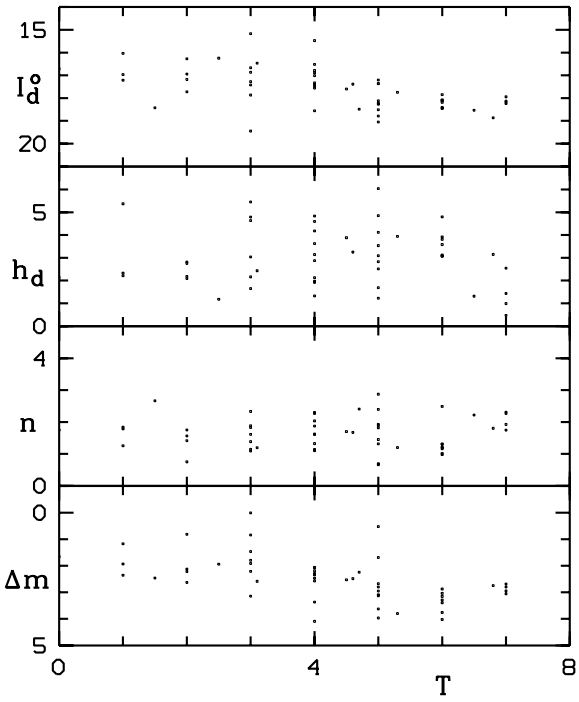

Fig. 5. Central surface brightness I_d^0 of the main disk, disk scale length h_d, Sérsic bulge index n, and bulge-to-disk ratio Δm as functions of the Hubble type T as given in RC3.

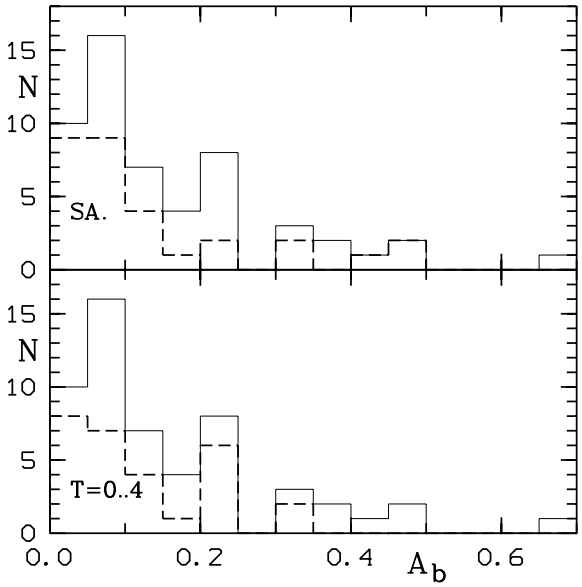

Fig. 6. Distribution of the mean relative amplitude of central bars. The total sample is shown by the full drawn line whereas ordinary SA. galaxies and early-type spirals are indicated by the dashed line.

the projection parameters of the main disk was included to simulate the effect of an oblate bulge. For ∼60% of the galaxies, the fitting procedure with a modified Hubble law indicated the present of a central point source while the number was less than 20% for the Sérsic law. If an inner disk was included, the fits were improved for 38 of the galaxies suggesting that many of the bulges are oblate.

The exponents n in Sérsic law had values mostly in the range 1−2 corresponding to either exponential or $r^{1/2}$ dependence as noted by Courteau (1996), de Jong (1996b) and Seigar & James (1998). There is no clear tendency for late-type spiral bulges to be more exponential, as seen in Fig. 5.

The fit of the $r^{1/n}$ law to the bulge depends somewhat on the assumed form of the PSF and the central point source (Trujillo et al. 2001). To provide a more stable estimate of the total bulge luminosity, the modified Hubble law was used, integrating up to 10 bulge scale lengths. The bulge to total luminosity ratio, expressed in magnitudes Δm, is given in Fig. 5 and shows only weak dependency on Hubble type as also noted by de Jong (1996b) in contrast to what is seen in visual colors (Simien & de Vaucouleurs 1986). The integrated luminosity of the central point source and inner disk is in all cases small compared to the bulge.

The fraction of ordinary spiral galaxies which show bar structures is significantly higher when observed in near-infrared bands (Eskridge et al. 2000; Seigar & James 1998) than it is in visual colors. This raise the question if bars or oval distortions are present at some level in all spiral galaxies or whether there exists a group of spirals without any bar distortions. Since bars may drive spiral structure (Sellwood & Sparke 1988; Lynden-Bell 1979), it is important to understand if there is any relation between bar-type perturbations and the spiral structure in a galaxy. The non-barred subsample was used to address these issues. It is expected that ordinary SA spirals would yield the lower part of the distribution of bar or oval perturbations.

The decompositions of the light distribution into disk and spheroid and correction for projection effects are critical issues for the detection of weak bar structures in spiral galaxies. If one bases oneself on the surface brightness distribution without a detailed velocity map of the central regions, it is impossible to distinguish between oblate spheroids, triaxial bulges and bars. To establish a lower limit for the number of weak bars in ordinary spirals, the bulge was assumed to be perfectly spherical and follow either a modified Hubble or Sérsic law. Galaxies with bulges which do not conform to these assumptions will exhibit artificial oval distortions as an effect of erroneous deprojection and subtraction of the spheroid. Thus, the derived values for the bar amplitudes are upper limits. It was not possible to detect small central bars with a relative amplitude of less than ∼3% due to problems of scattered light, pixel interpolation errors and uncertainties in the exact shape of the PSF.

The distribution of the mean relative amplitude of the $m = 2$ harmonic in the bar region is shown in Fig. 6. Besides the total histogram, the subsamples of ordinary SA galaxies and early-type spirals with $T < 5$ are given. Galaxies classified as ordinary have on average weaker bars than intermediate SX spirals, as expected; however, there is significant overlap. No oval distortion could be identified in 4 of the 30 SA galaxies at the 3% level while 10 had amplitudes of less than 5%. All 4 spirals with no detected bar were early-type SA galaxies. This suggests that truly non-barred galaxies do exist although in modest numbers. The current sample indicates that 10−15% of SA galaxies have no significant bar-like perturbation in their central parts which would correspond to around 5% of all spiral

galaxies. This is consistent with the fraction of non-barred galaxies found by Seigar & James (1998). Eskridge et al. (2000) classified 27% of their total sample of galaxies as non-barred in the H band. This significantly higher fraction is caused likely by the visual classification used with which a higher bar amplitude may be required for detection. The bar strength does not show any significant correlation with morphological type or bulge properties.

The bar amplitude, A_b, gives the relative light variation in the *K* band of the bar perturbation. This does not necessarily correspond to the dynamic importance which is better described by the gravitational torque (Combes & Sanders 1981; Buta & Block 2001).

Since the current sample is biased towards ordinary and intermediate barred spirals most bars are relative short. The bar size is mostly less than the disk scale length (see Table 2) whereas normal bars typically are longer. This makes it impossible to determine the detailed shape of the radial bar profiles. The azimuthal profiles are often sharper than a pure $m = 2$ harmonic as indicated by the presence of higher order even harmonics almost in phase with the bisymmetric perturbation.

The strength of the bars is given by the amplitude of the $m = 2$ harmonic as derived from the 1D Fourier analysis since it provides a stable measure which is little sensitive to noise. Seigar & James (1998) suggested to use the "equivalent angle" which also is a stable estimate and can be applied to individual azimuthal features. For a pure sinusoidal $m = 2$ perturbation, the "equivalent angle" is proportional to the relative amplitude A_2 if the disk is defined as the average intensity at the radius. To compare the two measures, the average equivalent angles for the bars were calculated using a polar map of the galaxies. This showed that the estimates were compatible and well correlated. The decomposition in Fourier coefficients was more natural for the analysis in terms of waves and was therefore preferred. A comparison with estimates of bar gravitational forcing (Buta & Block 2001) will be discussed in a forthcoming paper.

A majority of galaxies (at least 33 systems) has a symmetric, grand design, two-armed spiral pattern (main pattern) which starts just outside the end of the bar distortion and often breaks up into a multi-arm structure (outer pattern) in the outer parts of the galaxies. Only one spiral, NGC 4030, show a flocculent appearance while the remaining galaxies have a patchy, lopsided morphology, often with bright knots. In some cases, one sees phase shifts between inner and outer patterns which could suggest that they belong to different modes. The properties of these patterns differ significantly and this makes it necessary to treat them separately. The radial extent of the main spiral was defined to start at the point where the absolute pitch angle $|i|$ of the $m = 2$ harmonic became less than 40° and terminate where either the pitch angle changed significantly or the $m = 4$ harmonic displayed an increased amplitude and a phase offset relative to the two-armed spiral. The estimate of these two radii was done manually both on plots of Fourier coefficients and direct maps of the relative perturbations in the disk. The two methods agree well and indicated that the standard error was of the order of 3″. It was difficult to trace the spiral pattern in some late-type galaxies (e.g. IC 5041, NGC 1087, and NGC 1494) in the direct images due to asymmetric features which possibly are associated to star forming regions. One galaxy, NGC 4939, showed a set of symmetric arm sections or arcs in its central region. In this case, the main spiral was assumed to start just outside these structures.

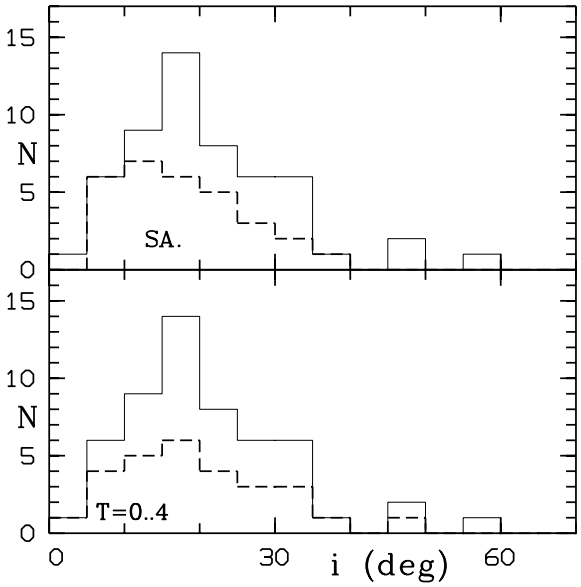

Fig. 7. Distribution of absolute values of the mean pitch angle for the main two-armed spiral pattern in the galaxies. The total sample is shown by the full drawn line while SA galaxies and early-type spirals are indicated by the dashed line.

The distribution of the absolute pitch angles is shown in Fig. 7 which also gives the subsets of SA and early-type spirals. The typical range is 5−35° with a tail of more open patterns. There is a weak tendency for galaxies classified as intermediate barred to have more open spirals than ordinary spirals. In addition, later Hubble types have, on average, arms that are more open, as expected from the classification criteria although the correlation is much weaker than the one found by Kennicutt (1981).

Amplitudes of the main two-armed spiral pattern as a function of its pitch angle are shown in Fig. 8. There is a lack of strong, tight patterns while there is a more even distribution of open spirals. It is difficult to detect spiral arms with pitch angles $|i_2| < 5$ degr due to their small radial inter-arm distances. The galaxies with higher relative amplitudes A_2 have been labeled in the figure. All of these have evidence of strong star formation in their arms and have therefore probably overestimated A_2 values.

The upper limit for the amplitude as a function of pitch angle can be approximated by the line $c \times \tan(|i_2|)$. This would be a natural consequence if the lack of strong, tight spirals was due to the radial forcing introduced by the spiral perturbations. Models of spiral galaxies indicate that non-linear effects become important if the relative radial force perturbation of the spiral exceed 5% (Grosbøl 1993). Spiral arms with stronger perturbations would be damped by non-linear effects.

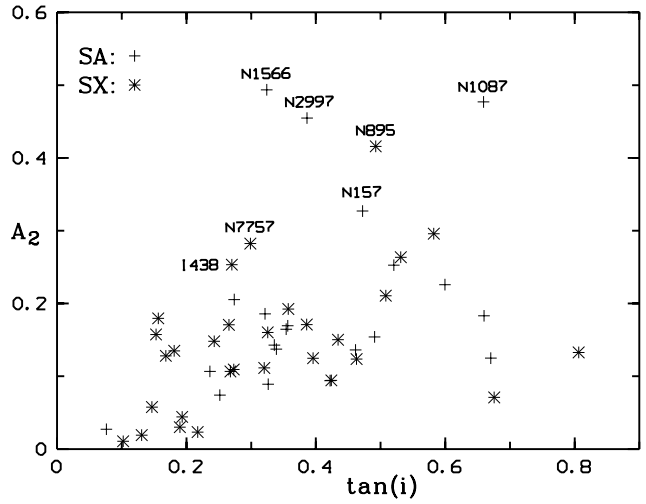

Fig. 8. The relative amplitude of the main $m = 2$ spiral as function of its absolute pitch angle.

7. Conclusions

The determination of accurate sky projection parameters for spiral galaxies is essential for the detailed study of their spiral structure. We find that the most stable estimate of the projection is obtained by minimizing the constant phase, $m = 2$ term of a 2D Fourier transform of a polar map of the main disk. This method is less sensitive to influence by spiral patterns and warps in the disk than direct 2D fits of an exponential disk.

The decomposition of the galaxies showed that most bulges were best approximated by an $r^{1/n}$ law with an index n in the range 1−2. The central surface brightness of the disk and the bulge-to-disk ratio showed only weak correlation with Hubble type. These results are in basic agreement with Courteau (1996), de Jong (1996a) and Seigar & James (1998). Indications of a central point source were found in many galaxies while more than 80% of them were better fitted adding a steep, inner exponential disk. This suggests that many bulges are oblate.

Weak bars and oval distortions with relative amplitudes down to ≈3% could be detected using Fourier transform techniques. Only 4 of the 30 ordinary spiral galaxies in the sample had no central bar perturbation at this level corresponding to 10−15% of the SA spirals, which is in agreement with Seigar & James (1998). The "equivalent angle" measure of bar strength used by these authors correlates well with the relative amplitude of the $m = 2$ Fourier component used in this paper.

A majority of the galaxies has a symmetric, grand design, two-armed spiral pattern in their inner parts which often breaks up into asymmetric, multi-armed branches in the outer parts. Phase shifts between the inner and outer pattern, seen in a few cases, suggest that they belong to different spiral modes. The absolute pitch angles of the main spiral show a typical range of 5−30°. There is a lack of strong, tight patterns. This is consistent with such spirals having a relative radial force perturbation high enough to make non-linear dynamics effects important, and therefore being damped.

Acknowledgements. We are very grateful for numerous fruitful discussions with Prof. G. Contopoulos and Dr. Ph. Héraudeau. The data for NGC 2997 and NGC 6118 were observed by Dr. A. Moorwood whom we thank for making them available to us. We also appreciate useful comments from the referee, Dr. D. L. Block. All image processing was done with the ESO-MIDAS system.

References

Barnes, E. I., & Sellwood, J. A. 2003, AJ, 125, 1164
Bertin, G., Lin, C. C., Lowe, S. A., & Thurstans, R. P. 1989, ApJ, 338, 78
Binney, J., & Tremaine, S. 1987, Galactic Dynamics (Princeton: Princeton Univ. Press)
Block, D. L., & Puerari, I. 1999, A&A, 342, 627
Block, D. L., & Wainscoat, R. J. 1991, Nature, 353, 48
Block, D. L., Bertin, G., Stockton, A., et al. 1994, A&A, 288, 365
Bottinelli, L., Gouguenheim, L., Paturel, G., & de Vaucouleurs, G. 1984, A&AS, 56, 381
Buta, R., & Block, D. L. 2001, ApJ, 550, 243
Buta, R., & Purcell, G. B. 1998, AJ, 115, 484
Buta, R., Block, D. L., & Knapen, J. H. 2003, AJ, 126, 1148
Caon, N., Capaccioli, M., & D'Onofrio, M. 1993, MNRAS, 265, 1013
Clemens, M. S., & Alexander, P. 2001, MNRAS, 321, 103
Combes, F., & Sanders, R. H. 1981, A&A, 96, 164
Contopoulos, G., & Grosbøl, P. 1986, A&A, 155, 11
Courteau, S. 1996, ApJS, 103, 363
Danver, C.-G. 1942, Ann. Obs. Lund, 10
de Jong, R. S. 1996a, A&AS, 118, 557
de Jong, R. S. 1996b, A&A, 313, 45
de Vaucouleurs, G. 1959, in Handbuch der Physik, ed. S. Flügge (Berlin: Springer-Verlag), 53, 275
de Vaucouleurs, G., de Vaucouleurs, A., Cowien, H., et al. 1991, Third reference catalogue of bright galaxies (New York: Springer)
Elmegreen, D. M., & Elmegreen, B. G. 1987, ApJ, 314, 3
Eskridge, P. B., Frogel, J. A., Pogge, R. W., et al. 2000, AJ, 119, 536
Freeman, K. C. 1970, ApJ, 160, 811
Garcia, A. M. 1995, A&A, 297, 56
Grosbøl, P. 1985, A&AS, 60, 261
Grosbøl, P. 1993, PASP, 105, 651
Grosbøl, P., & Patsis, P. A. 1998, A&A, 336, 840
Hameed, S., Blank, D. L., Young, L. M., & Devereux, N. 2001, ApJ, 546, L97
Honma, M. 1999, ApJ, 516, 69
Jarrett, T. H., Chester, T., Cutri, R., et al. 2000, AJ, 119, 2498
Karachentsev, I. D., Grebel, E. K., Sharina, M. E., et al. 2003, A&A, 404, 93
Kennicutt, R. C. 1981, AJ, 86, 1847
Kent, S. M. 1985, ApJS, 59, 115
Klimanov, S. A., & Reshetnikov, V. P. 2001, A&A, 378, 428
Laine, S., Shlosman, I., & Heller, C. H. 1998, MNRAS, 297, 1052
Lin, C. C., & Shu, F. H. 1964, ApJ, 140, 646
Lin, C. C., & Shu, F. H. 1966, Proc. Natl. Acad. Sci. USA, 55, 237
Lynden-Bell, D. 1979, MNRAS, 187, 101
Merrifield, M. R., & Kuijken, K. 1995, MNRAS, 274, 933
Patsis, P. A., & Athanassoula, E. 2000, A&A, 358, 45
Patsis, P. A., Héraudeau, P., & Grosbøl, P. 2001, A&A, 370, 875
Persson, S. E., Murphy, D. C., Krzeminski, W., Roth, M., & Rieke, M. J. 1998, AJ, 116, 2475
Peterson, C. J. 1978, ApJ, 226, 75
Pompei, E., & Pérez, I. 1999, Ap&SS, 269, 659

Reynolds, J. H. 1924, MNRAS, 85, 142
Rix, H.-W., & Rieke, M. J. 1993, ApJ, 418, 123
Roberts, W. W., Roberts, M. S., & Shu, F. H. 1975, ApJ, 196, 381
Ryder, S. D., Zasov, A. V., McIntyre, V. J., Walsh, W., & Sil'chenko, O. K. 1998, MNRAS, 293, 411
Sandage, A., & Bedke, J. 1994, The Carnegie Atlas of Galaxies, Carnegie Inst. of Wash. Publ. No. 638 (Washington: Carnegie Inst.)
Seigar, M. S., & James, P. A. 1998, MNRAS, 299, 672
Sellwood, J. A., & Sparke, L. S. 1988, MNRAS, 231, 25
Sérsic, J. L. 1968, Atlas de galaxias australes (Cordoba: Obs. Astron. de Cordoba)
Simien, F., & de Vaucouleurs, G. 1986, ApJ, 302, 564
Soares, D. S. L., de Souza, R. E., de Carvalho, R. R., & Couto da Silva, T. C. 1995, A&AS, 110, 371
Trujillo, I., Aguerri, A. L., Cepa, J., & Gutiérrez, C. M. 2001, MNRAS, 321, 269
van den Bergh, S. 1960a, ApJ, 131, 558
van den Bergh, S. 1960b, ApJ, 131, 215
van der Kruit, P. C. 1987, A&A, 173, 59
Wainscoat, R. J., & Cowie, L. L. 1992, AJ, 103, 332
Zaritsky, D., & Rix, H.-W. 1997, ApJ, 477, 118
Zaritsky, D., Smith, R., Frenk, C., et al. 1997, ApJ, 478, 39

Online Material

Appendix A: Individual galaxies

Spiral arms in many disk galaxies display individual morphological features that can be described only partly by parameterization (e.g. as coefficients of a Fourier transform) due to their high spatial frequencies and irregular nature. Although the K'-band images have a much smoother appearance than optical maps, they still frequently show knots along the spiral arms and inter-arm features. The relative weak perturbations in the disks compared to the exponential decrease of their surface brightness makes it difficult to distinguish spiral features on direct images. Thus, maps giving intensities normalized to the mean radial profile of the galaxies were used for visual inspection. For each galaxy two representations are displayed in Figs. A.1–A.6, namely a direct face-on view and a logarithmic polar map which makes it easier to follow logarithmic spiral perturbations. A starting radius of 3″ was adopted although this made it necessary to interpolate between pixels for the smallest radii.

A brief description of the main features for each galaxy is given below.

IC 0438. A grand-design galaxy with an insignificant bar. The inner symmetry of the spiral pattern breaks as the pitch angle of one of the arms changes abruptly at 24″. The deprojected relative map reveals a multi-arm structure beyond a radius of 49″.

IC 5020. A weakly barred, multi-armed galaxy. A two-armed spiral pattern is observed in the central part.

IC 5041. Practically just a galactic bar. Close to the end of the bar one can observe arcs of enhanced intensity, which could be considered as the beginning of a weak spiral pattern. Forms a pair with IC 5039 (Honma 1999).

IC 5332. Rather faint arms, but grand-design spiral morphology. A bar-like feature can be observed at radii less than 10″. There is a smooth transition between the bar and the spiral pattern giving it a typical s-shaped morphology.

NGC 157. A well known grand-design spiral with strong star formation in the arms. A weak bar is identified in its central regions. The rotation curve is rising over the whole region where the spiral pattern exists (Ryder et al. 1998). The very inner part may be affected by an incorrect bulge subtraction.

NGC 173. A ring-type, barred galaxy with strong arms with outer faint extensions, discernible only in the deprojected relative map.

NGC 210. This galaxy is characterized by a bar with an inner twist and a thin faint pair of very open spiral arms in its outer parts.

NGC 470. A bar structure is clearly seen in the galaxy although it was classified as SA(rs)b in RC3. At the end of the bar a ring-like structure appears to which the spiral pattern is attached.

NGC 488. A typical early-type spiral galaxy with very tightly wound spirals. Nevertheless, in the deprojected relative map we can observe a central barred component. Zaritsky et al. (1997) mentions three satellites. Two of them rotate in a retrograde orbit and one in prograde orbits around the galaxy.

NGC 578. A grand-design barred galaxy, with characteristic star forming activity along the spiral arms.

NGC 685. The galaxy has a prominent bar with faint spiral arms attached to it. The arms contain many bright knots suggesting recent star formation.

NGC 787. Faint, weakly barred galaxy with anemic asymmetric spiral structure.

NGC 895. Very open bisymmetric spiral. The pitch angle decreases towards the central part. A bar-like feature is present.

NGC 897. A galaxy with remarkable morphological similarity to NGC 488 with a very weak bar. Zaritsky & Rix (1997) mention again three satellites (2 in prograde and 1 in retrograde orbits) of the galaxy. The very inner part may be affected by an incorrect bulge subtraction.

NGC 1068. Barred, ringed, with bisymmetric spiral arms. Strong star formation is observed both in the bar and in the spiral arms.

NGC 1087. Very open, extended spiral pattern with a central bar component. Many bright knots are seen.

NGC 1137. The main morphological feature discernible is a central bar. It is surrounded by a patchy spiral pattern.

NGC 1255. An s-shaped barred spiral galaxy. In the outer disk we observe numerous star-formation regions.

NGC 1309. S-shaped, lopsided galaxy with many young objects along the spiral arms.

NGC 1357. Grand-design with wound, narrow, bright spiral arms. There may be a weak oval distortion inside the spiral. Close to the inner limit of the spiral pattern a ring can be observed.

NGC 1371. S-shaped, barred galaxy. The bar ends in two symmetric, high intensity regions which form the transition to the spiral.The spiral is asymmetric. This galaxy has a triaxial bulge (Pompei & Pérez 1999).

NGC 1494. The spiral pattern is weak and asymmetric. The galaxy has a fuzzy central region. No significant bulge component is present as mentioned by Sandage & Bedke (1994).

NGC 1566. Another well known, grand-design spiral galaxy. The deprojected relative map clearly shows the presence of a central bar component which is not aligned with the innermost points of the spiral. The arms show strong star formation.

NGC 2618. Galaxy with a weak inner bar, a possible ring and a wound spiral pattern.

NGC 2775. An Sa galaxy with a bar component embedded in the bulge region. The spiral pattern has two components which partly overlap, namely: an inner tight spiral and an outer more open pattern. The latter was traced by the 1D Fourier analysis.

NGC 2855. This galaxy is characterized by the presence of shells. Apparently a remnant of an interaction.

NGC 2997. A grand-design spiral galaxy with the bisymmetric spiral pattern attached to a bulge with an oval distortion. The central region contains a ring of hot spots. The spiral arms have many bright knots indicating strong star formation.

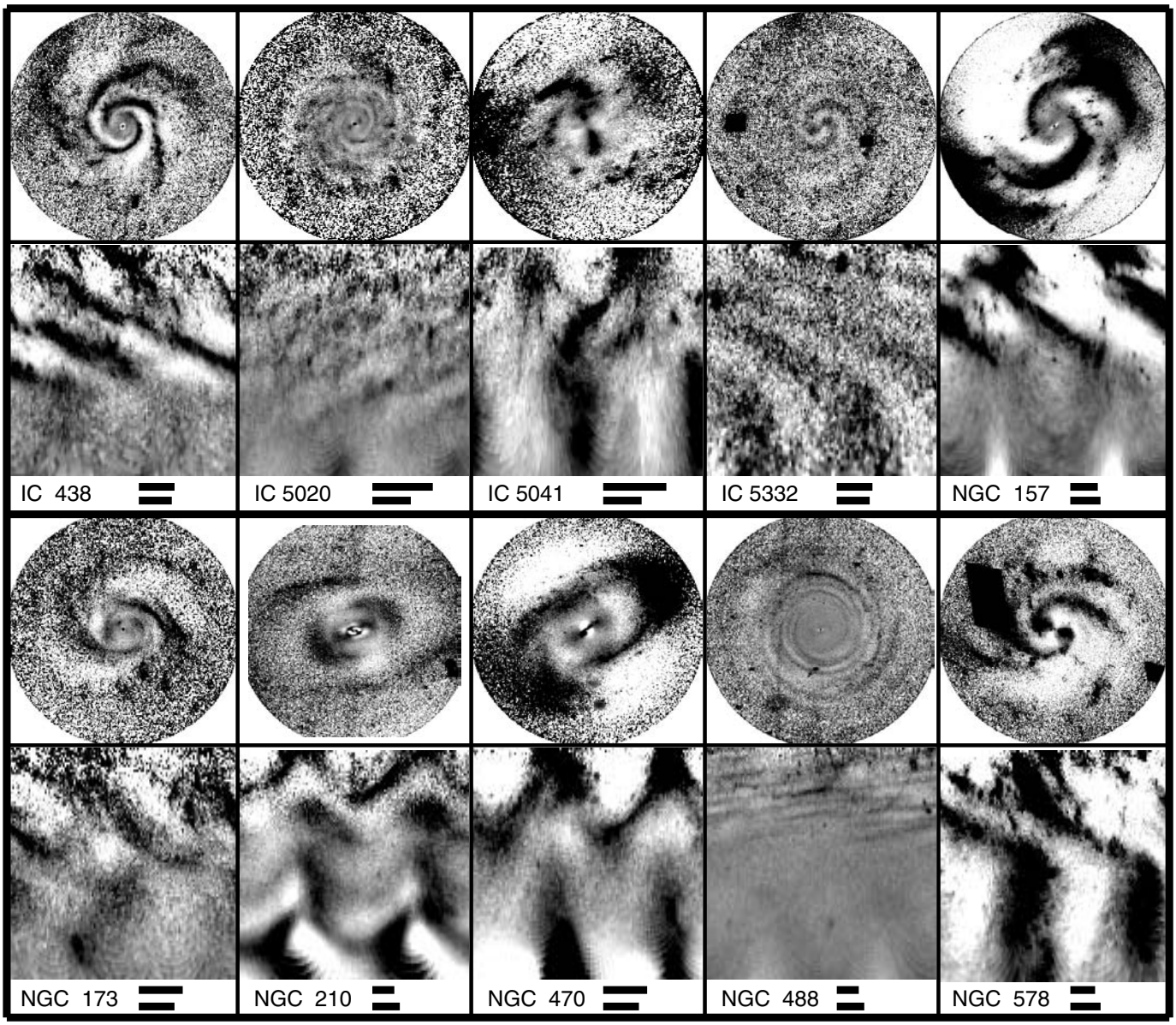

Fig. A.1. Relative perturbations in the disks of galaxies in the sample. Bulge and foreground stars were subtracted. For each galaxy both direct face-on and θ-ln(r) maps are shown. The scale is indicated by the two bars which represent 30″ for the direct image (*upper*) and 0.5 for the logarithmic map (*lower*). The abscissa in the θ–ln(r) diagrams gives the azimuthal angle in the range 0–2π counting from the major axis. The range shown covers ±30% in negative representation where dark indicate excess of light.

NGC 3054. The central region has a Θ- type morphology, i.e. a bar surrounded by a ring. Four bright regions close to the ring are offset by 90° from each other. There is a clear bisymmetric part of the spiral pattern, and further out several segments of spiral arms.

NGC 3173. A barred galaxy with anemic spiral arms, hardly traced even in the relative map.

NGC 3241. The central region has a Θ-type morphology with sets of bisymmetric bright regions offset by 90°. The spiral pattern may have four arms.

NGC 4030. The galaxy has a flocculent appearance with multiple spiral arms in its central region. In the outer parts, a two-armed pattern prevails. A weak bar may be present in the very center.

NGC 4653. A weakly barred, grand-design spiral, with a main bisymmetric spiral pattern. This pattern also has weak extensions to larger radii. A phase shift of the spiral pattern can be seen between the weaker inner part and the strong outer section.

NGC 4713. Barred galaxy with an asymmetric spiral pattern, characterized by the presence of numerous bright knots in the arms and the inter-arm regions.

NGC 4939. This galaxy is characterized by sets of almost symmetric arcs with respect to the center, which probably reflects the presence of families of periodic orbits. Each set of arcs is offset by 90°. Further out there is a bisymmetric spiral pattern.

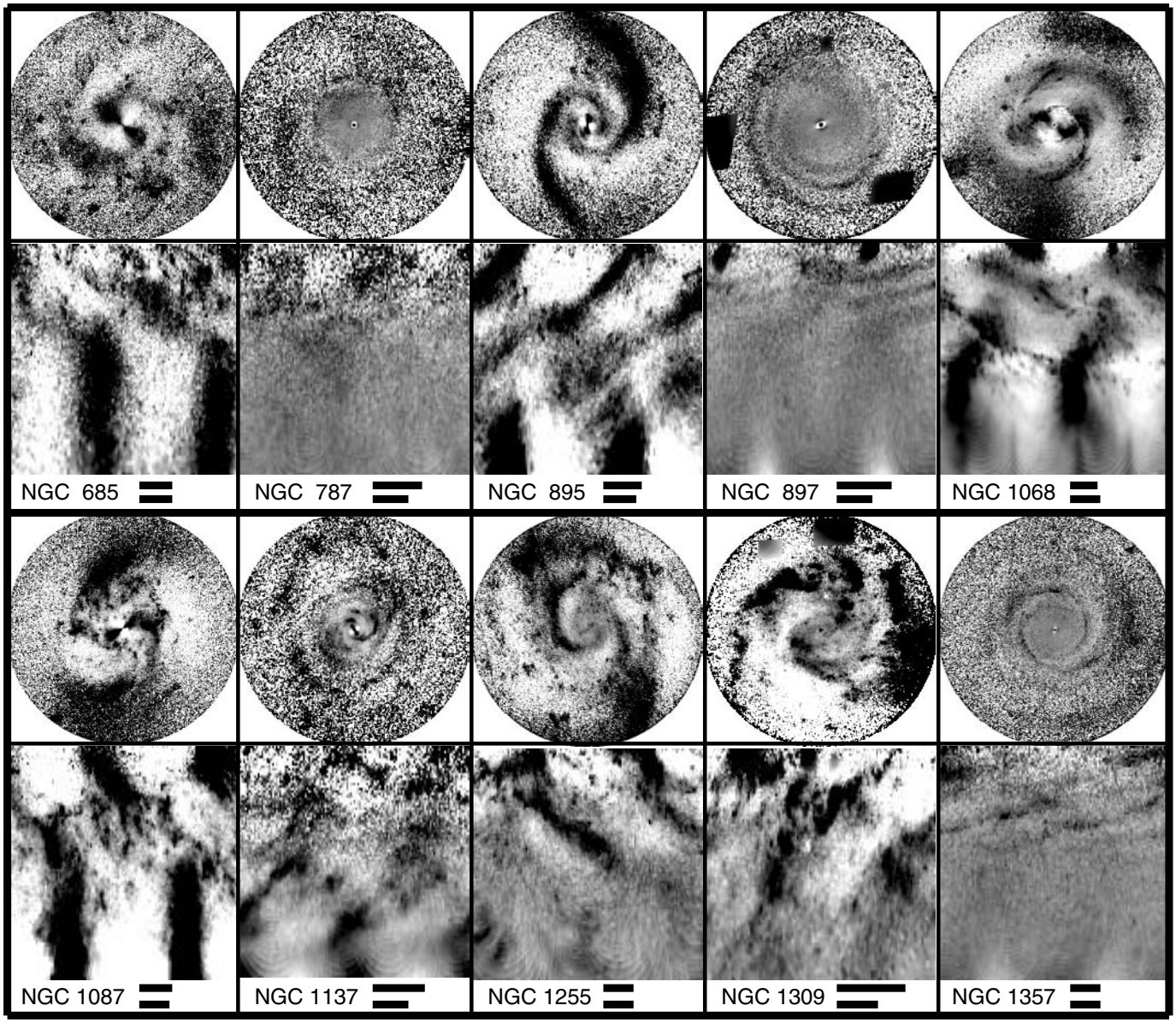

Fig. A.2. Relative perturbations in the disks of spiral galaxies shown as direct and θ–ln(r) maps as in Fig. A.1.

NGC 4941. A barred galaxy accompanied by two asymmetric spiral arms. The very inner part may be affected by an incorrect bulge subtraction.

NGC 4965. A lopsided weak spiral with many bright knots all over the disk.

NGC 4981. Grand-design, barred galaxy with a bisymmetric spiral pattern, which in the outer regions of the disk splits in several segments of spiral arms.

NGC 5300. Apparent weak spiral although the *K* map of this galaxy had the worst SNR in the sample. Elmegreen & Elmegreen (1987) attribute to it an arm class 2.

NGC 5643. A typical strong bar case. Open spiral arms are attached to the end of the bar. One can observe the "T"-shaped regions at the end of the bar modeled by Patsis & Athanassoula (2000).

NGC 5688. A ringed barred galaxy with a weak spiral. Two bar structures with a phase offset are seen.

NGC 5806. An asymmetric spiral pattern and a central bar which does not join the inner start of the spiral. The inner part may be affected by an incorrect bulge subtraction.

NGC 6070. Barred, two-armed galaxy with several inter-arm spurs. The bar appears to have a complex internal structure. Many bright knots are seem, mainly in the arms.

NGC 6118. A grand-design spiral, with a very small central bar that makes a smooth transition to a spiral pattern with an s-shaped morphology. A characteristic increase of the pitch angle occurs at $r \approx 22''$. This suggest the presence of a resonance at that distance. In the outer regions of the disk the spiral pattern splits.

NGC 6384. A Θ-type central morphology. Multiple spiral arms with bright knots, mainly in the arms.

NGC 6902. A weak inner bar is present with two intensity enhancements offset by 90° just outside. There seems to be a bridge between the end of the bar and the enhancements

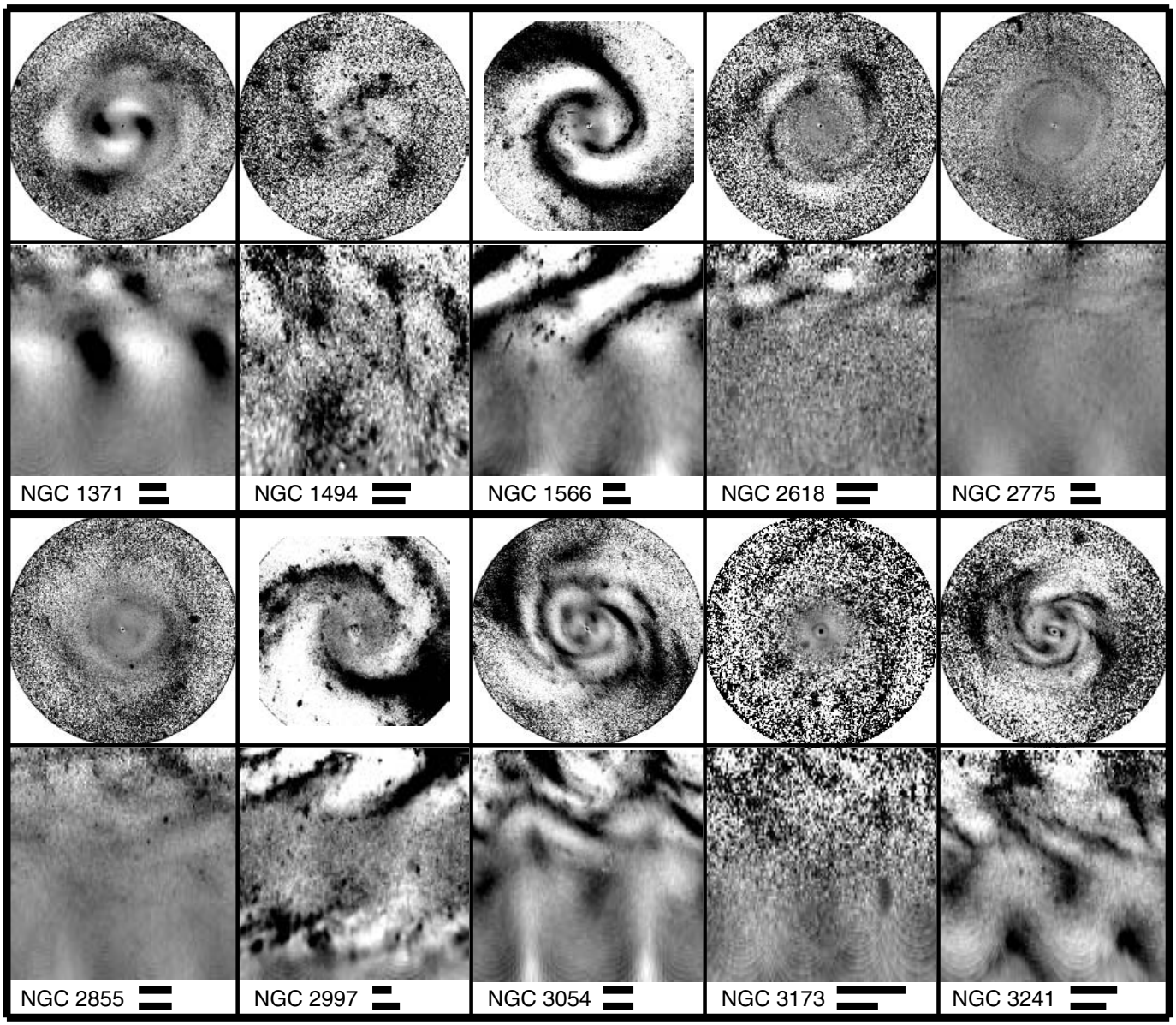

Fig. A.3. Relative perturbations in the disks of spiral galaxies shown as direct and θ–ln(r) maps as in Fig. A.1.

which could be interpreted as a short spiral pattern winding in the opposite sense to the narrow, tight arms starting just outside. It belongs to a compact group of galaxies (Garcia 1995).

NGC 7070. A barred galaxy with thin spiral arms with "corners". The outer spiral pattern is asymmetric.

NGC 7125. Ringed galaxy with lopsided spiral arms with many bright knots. Inside the ring there is an inner bar. It forms a pair with NGC 7126 (Honma 1999).

NGC 7213. An Sa galaxy with a very tight, weak spiral. Hameed et al. (2001) argue that the H I map reveals this galaxy to be a highly disturbed system, suggesting a past merging event.

NGC 7392. A strong bar with "T" regions, ring, and a quite symmetric outer spiral pattern. The inner part may be affected by an inadequate bulge subtraction.

NGC 7418. Barred galaxy with an asymmetric two-armed spiral with several inter-arm spurs. Many bright knots are present. Bar and inner end of spiral are not aligned.

NGC 7637. Very weak bar, if any, but strongly lopsided center. Patch, arm segments which go into a single outer arm. Member of a galaxy pair according to Soares et al. (1995).

NGC 7757. S-shaped, barred galaxy with thin spiral arms with many bright knots. It has a companion and for this reason it is characterized by Klimanov & Reshetnikov (2001) as an "M 51"-type object.

NGC 7793. Bar and spiral structure are difficult to trace as the galaxy is resolved into individual stars. It is one of the five well-known galaxies making up the nearby Sculptor galaxy group.

UGC 1167. S-shaped, weakly barred galaxy with a grand-design inner spiral with segments of spiral arms extending

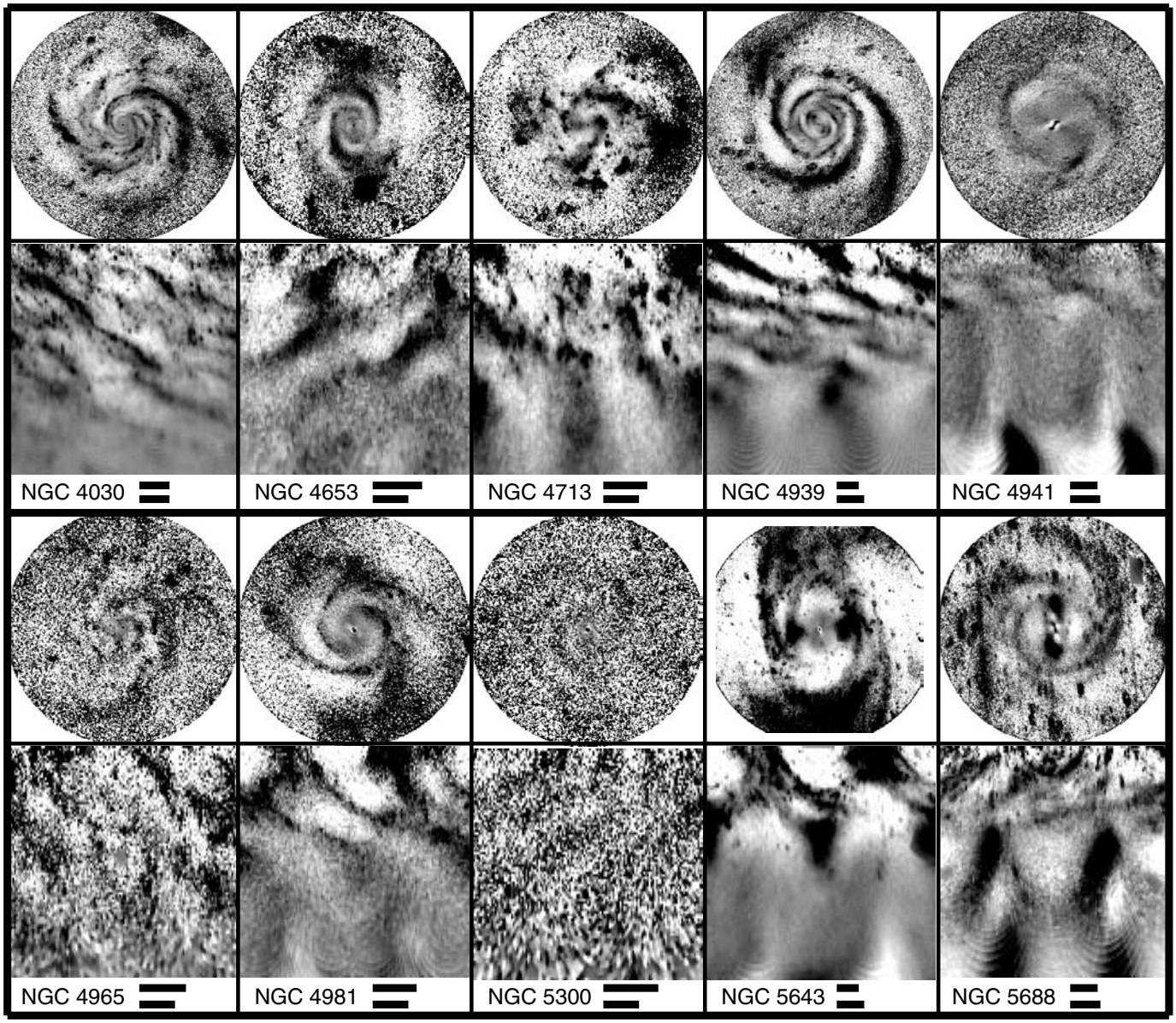

Fig. A.4. Relative perturbations in the disks of spiral galaxies shown as direct and θ–ln(r) maps as in Fig. A.1.

to larger distances. There seems to be a phase shift in the spiral pattern.

The majority of the galaxies ($33/54 \approx 61\%$) has a two-armed grand-design spiral pattern in their inner parts while multi-armed spiral structures dominate in the outer regions in at least $10/33 \approx 30\%$ of these galaxies. The transition between bar and spiral is smooth, s-shaped in $14/54 \approx 26\%$ of the galaxies whereas the majority ($33/54 \approx 61\%$) displays either an abrupt change of pitch angle or a ring type structure. Several galaxies (at least $6/54 \approx 11\%$) have a complex central structure with several sets of bars, arcs or spirals.

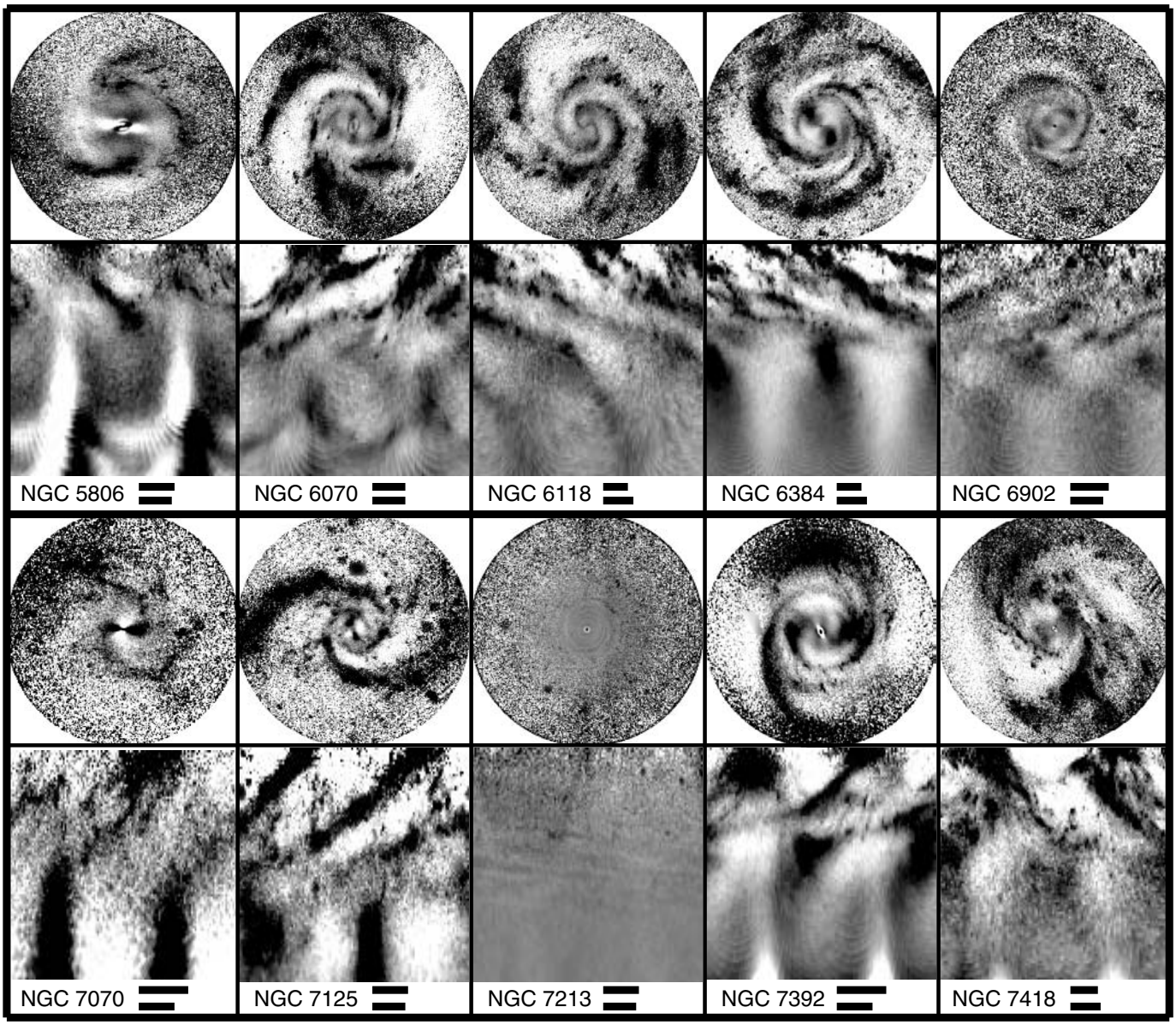

Fig. A.5. Relative perturbations in the disks of spiral galaxies shown as direct and θ–ln(r) maps as in Fig. A.1.

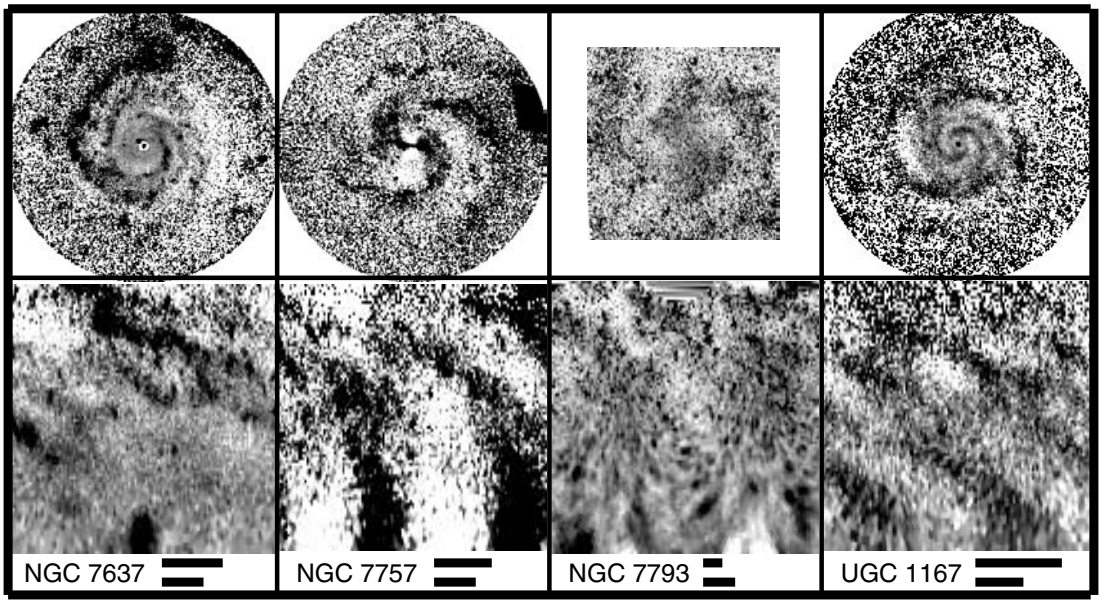

Fig. A.6. Relative perturbations in the disks of spiral galaxies shown as direct and θ–ln(r) maps as in Fig. A.1.